# Design and Performance of a Compact $Cs_2LiLaBr_6(Ce)$ Neutron / Gamma Detector Using Silicon Photomultipliers

Peter R. Menge, *Member, IEEE*, Julien Lejay, and Vladimir Ouspenski

***Abstract*– $Cs_2LiLaBr_6(Ce)$ (CLLB) crystal scintillator shows great potential as a radiation detection material with excellent energy resolution for gammas, sensitivity to neutrons, and the ability to separate the two using pulse shape discrimination (PSD). Experiments have been performed testing this material using silicon photomultipliers for creation of compact, easily-portable detectors for dual gamma ray spectroscopy and neutron detection. Pulse shape discrimination in CLLB is achieved by analyzing the scintillation pulse decay on the time scales of >1 μs. This feature enables the silicon photomultipliers with low afterpulsing to achieve suitable discrimination. Experiments have been conducted attempting to find a suitable cost/efficiency compromise that maximizes performance by varying crystal cerium concentration along with silicon photomultiplier type and placement position. A disk of CLLB (diameter = 52 mm, thickness = 6 mm, $^6$Li enriched) coupled to a 6x6 mm$^2$ silicon photomultiplier can achieve 4.4% gamma ray energy resolution at 1275 keV, and 74% thermal neutron detection efficiency with a high pulse shape discrimination figure-of-merit of 1.9.**

## I. Introduction

COMPACT, lightweight, hand-portable radiation detectors are necessary for many nuclear security applications including active search and passive monitoring for isotope identification and fissile material detection. A desirable instrument would combine a dual-mode detection material with a solid state read-out to create an extremely compact, power efficient, and easy-to-carry device. A good choice for such a device is to combine the scintillator, $Cs_2LiLaBr_6$:Ce (CLLB), with a silicon photomultiplier (SiPM) light sensor. Table I lists pertinent performance characteristics of CLLB crystal scintillator.

TABLE I. CLLB PERFORMANCE CHARACTERISTICS

| Parameter | Typical Value |
|---|---|
| Energy resolution | 3.1% at 662 keV on PMT |
| Light yield | 45,000 photons/MeV |
| Decay time | 180 and 1140 ns |
| Emission peak | 420 nm |
| Thermal neutron abs. length | 3 mm with 95% $^6$Li |

Manuscript received November 23, 2015. This work was supported in part by the U.S. Defense Advanced Research Projects Agency under Contract No HR0011-15-C-001.

Peter R. Menge is with Saint-Gobain Crystals, Hiram, OH 44234 USA (telephone: 440-834-5673, e-mail: peter.r.menge@saint-gobain.com).

Julien Lejay and Vladimir Ouspenski are with Saint-Gobain Recherché, 93303 Aubervilliers Cedex, France.

When enriched with $^6$Li, CLLB is an efficient neutron detector with a thermal neutron absorption length of less than 3 mm. When measured on a photomultiplier tube (PMT), CLLB has also shown excellent gamma ray detection ability with an energy resolution as low as 2.9% at 662 keV [1]. The ability to discriminate between gamma rays and neutrons via pulse shape has been shown to be suitable [2],[3].

SiPMs are available from several manufacturers, have been rising rapidly in performance over the last few years and are now approaching the performance of PMTs in several applications. Their attractiveness for creating compact detectors is obvious. When compared to PMTs, they use 20x less power, take up 1000x less volume, and use low voltage (<60 V). One drawback is that single SiPMs are small in size and cannot cover a significant area of the crystal, which can lead to non-uniformity in light collection and degradation of signal-to-noise. SiPMs may be tiled together to increase area coverage, but then gain variation among the tiles could worsen energy resolution.

Several considerations must be addressed to create the best performing device possible while keeping the detector compact and not too expensive. The detector size goal for this project is to keep the whole device prototype under 250 cm$^3$ with an aspect ratio similar to a cell-phone (e.g. 2x6x15 cm$^3$). The design considerations are the Ce activator level in CLLB, the size and shape of the CLLB detector crystal, the size, placement and manufacturer of the SiPM sensor.

Discrimination between gamma rays and neutrons is done by pulse shape discrimination (PSD). The scintillation pulse created by the energy deposition from neutron reaction products [i.e. from $^6$Li(n,t)α] is faster than that created by gamma rays [1]. Fig. 1 shows example pulses from neutron and gamma ray events taken with a photomultiplier tube (Hamamatsu R6233). Note that the greatest difference between the pulses occurs late in time when the photon flux is only a few photon/ns.

The decay of the pulses in Fig. 1 can be modeled by a double exponential fit. Table II lists the decay components and the fraction of the total light contained in each component. Note that pulses from neutron reactions produce more light in the fast component.

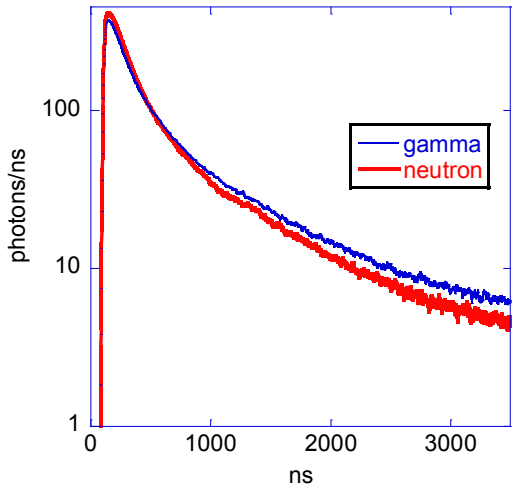


Fig. 1. Scintillation pulses corresponding to gamma ray and neutron reactions. Each waveform is an average of 50 pulses corresponding to 3.1 MeVee.

TABLE II. CLLB DECAY TIME COMPONENTS

| Reaction | $\tau_{fast}$ | $\tau_{slow}$ |
|---|---|---|
| Gamma Ray | 180 ns (40%) | 1140 ns (60%) |
| Neutron | 180 ns (50%) | 1140 ns (50%) |

Fig. 2 shows a density-contour plot of the ratio of the amount of light at the beginning of the pulse to the amount of light at the end versus the total amount of light in the pulse. The contours indicate the relative number of pulses recorded in each pixel of the plot. Specifically, the ordinate value is determined by the signal integral windows ratio:

$$\text{Head/tail} = \frac{\int_{tp}^{tp+150ns} S(t)dt}{\int_{tp+700ns}^{tp+2900ns} S(t)dt}, \quad (1)$$

where tp is the time at the peak of the pulse, and S(t) is the PMT signal at time t. Specifically, the abscissa is

$$\text{Energy} = \int_{tp}^{tp+3500ns} S(t)dt \quad , \quad (2)$$

The center of the feature labeled as "neutrons" corresponds to 3.1 MeV gamma equivalent energy. Note the excellent separation between the neutron region and the gamma ray region. The value for the PSD figure-of-merit (PSD FoM) is 2.0 when calculated for energies above 2.8 MeV [4]. A rule-of-thumb is that when the PSD FoM is greater than 1.5, then for most practical purposes, complete separation of gammas and neutrons can be obtained [5].

## II. DESIGN CHOICES

### A. Crystal Composition Size and Shape

The first design choice to be made is the size and shape of the CLLB crystal. The thermal neutron absorption length in CLLB enriched with 95% $^6$Li is 3 mm. The absorption length for a 662 keV gamma ray is 30 mm. Common detection targets usually emit far more gamma rays than neutrons. Thus, the ideal neutron detector is small in thickness but large in area. The ideal gamma detector is large in thickness and area. Unfortunately, creating a detector that is large in area, thick and inexpensive is not possible with CLLB (nor with other high performance scintillators).

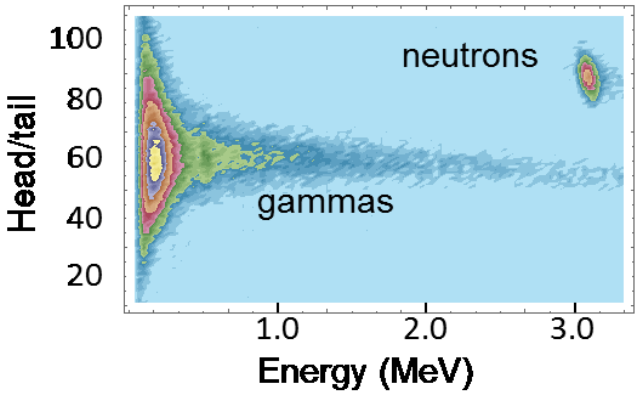


Fig. 2. PSD density contour plot for CLLB scintillation waveforms on a PMT and under irradiation from a moderated $^{252}$Cf source.

Saint-Gobain currently grows CLLB in cylindrical ingots that are diameter = 2 – 3 in. with a length of a few inches. The most cost effective means of producing detector crystals is to cut disks with the same diameter as the ingot. This minimizes wasted crystal containing expensive $^6$Li compound. A CLLB disk with diameter (Ø) = 52 mm and thickness (h) = 6 mm was chosen as giving the optimum performance per unit cost.

In CLLB, the performance changes with the Ce activator concentration [1]. Energy resolution improves when the amount of Ce is relatively high, but PSD FoM improves when the amount of Ce is relatively low. Table III lists experiments performed on disks with varying [Ce]. For these tests, the crystal edge was coupled to the PMT. For each crystal, a flat 6x6 mm$^2$ region was ground into edge of the disk, and this flat region was optically coupled to the PMT with silicone grease. The crystal disk was illuminated from the face side with a $^{137}$Cs gamma ray source. The purpose of using this unusual crystal-to-PMT coupling geometry will be made clear in the next section. Inspection of Table III shows that using a Ce concentration of 2 mol.% provides the best combination of energy resolution and PSD performance.

TABLE III. CLLB PERFORMANCE VERSUS [CE]

| [Ce] | Energy res. at 662 keV* | PSD FoM |
|---|---|---|
| 2% | 4.5 ± 0.3% | 1.9 ± 0.1 |
| 5% | 4.3 ± 0.2% | 1.4 ± 0.2 |
| 10% | 4.4 ± 0.3% | 1.2 ± 0.3 |
| 20% | 5.8 ± 0.4% | 0.8 ± 0.1 |

*measured with the edge of the crystal disk coupled to the PMT

### B. SiPM Type and Placement

Upon the selection of the Ø=52mm, h=6mm disk scintillator geometry with [Ce] = 2 mol.%, the next step is to decide where on the disk to place the SiPM(s). Two obvious choices are on the 6 mm edge or in the center of one circular face. Optical simulations were run to determine this design issue [6], [7]. Fig. 3 shows the result of three example

simulations with a 6x6 $mm^2$ SiPM placed on the center face, on the edge, and in both locations simultaneously. The simulations included assuming the crystal was surrounded by diffuse PTFE reflector and had a slightly roughened surface. The schematics in the lower right quadrant of Fig. 3 show notional diagrams of the SiPM placements on the crystal disks. The plots in Figs. 3a – 3c are contour density maps of the light collection probability (LCP). Scintillation pulses containing many thousands of photons were generated with uniform spatial distribution and allowed to optically propagate through the system. The relative probability of being detected by the SiPM as a function of position of origin is shown in the plots. The brighter the color, the greater the probability of detection. The more uniform the color, the greater the uniformity of light collection. When the SiPM is placed in the center face position, a greater fraction of the light is collected from interactions occurring directly underneath the sensor (Fig. 3a). Interestingly, when the SiPM is placed on the edge, light from around the entire periphery is collected more efficiently than light from the center (Fig. 3b). This is due to the fact that light created closer to the periphery will (on average) intersect the edge at more oblique angles. The probability for Fresnel reflection or total-internal reflection is higher for these photons, and thus, they are less likely to be absorbed by the surrounding reflector. The configuration of Fig. 3c attempts to harness the complementarity of the other two by using both configurations together.

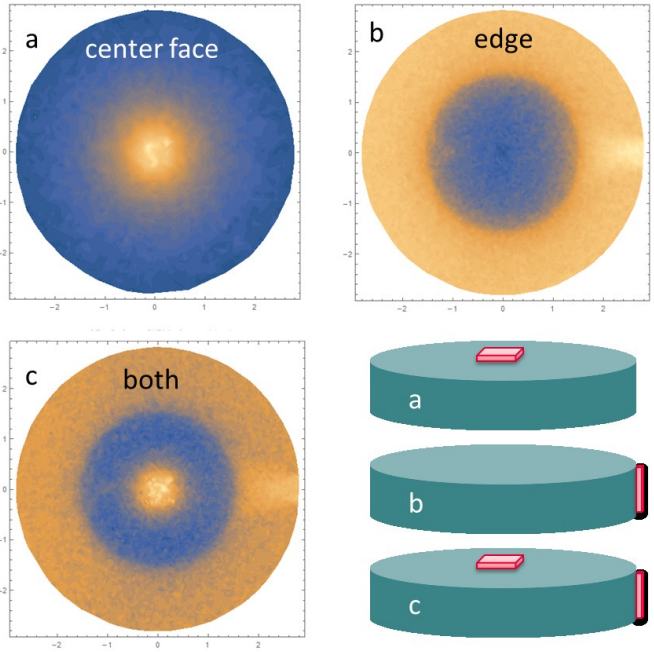


Fig. 3. Optical simulation results showing light collection probability maps for three example SiPM placement positions.

Non-uniformity in light collection worsens the energy resolution. The full width at half maxima (fwhm) of the LCP distributions for several simulations are shown in Table IV along with their experimental analogs. The results of the simulations shown in Fig. 3 are entries 2, 4, and 6 in Table IV. The experimental data were collected using the same crystal and SIPM models (SensL C-series, p-on-n type with high spectral sensitivity in the blue region corresponding to CLLB emission). The fwhm of the LCP distribution adds in quadrature with the other processes that lead to broadening of the energy resolution such as the intrinsic resolution and Poisson statistics [8]. Thus, it is desirable to have the fwhm of the LCP as narrow as possible. Note from Table IV, that the best uniformity is achieved with SiPMs on both the face and the edge. However, this configuration is only marginally better than using one SiPM on the edge. Thus, the detector design is to use only the edge configuration to reduce cost and complexity.

TABLE IV. EFFECT OF SIPM PLACEMENT ON LCP AND ERES

| SiPM size | SiPM placement | Simulated LCP fwhm | Measured energy resolution at 1275 keV |
|---|---|---|---|
| 3x3$mm^2$ | center face | 3.8% | 7.5% |
| 6x6$mm^2$ | center face | 3.2% | 6.0% |
| 3x3$mm^2$ | edge | 2.9% | 6.9% |
| 6x6$mm^2$ | edge | 2.6% | 5.0% |
| 12x6$mm^2$ | edge (2 abutted) | 2.2% | 4.9% |
| 6x6$mm^2$ | center face & edge | 2.1% | 4.8% |

Looking at Fig. 1, one can see that it is important to use an SiPM with enough signal-to-noise (S-to-N) late in the scintillation pulse to differentiate between gamma ray and neutron signals. Unfortunately, in addition to dark counts and cross-talk, SiPMs can suffer from a type of noise called afterpulsing, which can be especially problematic for the PSD function in CLLB. In SiPMs, afterpulsing results from charge carriers that are trapped on silicon defects and then thermally released at later times [9]. When released, the un-trapped charge carrier produces another microcell avalanche, which looks like the detection of another photon. Afterpulsing occurs at random times following the initial pulse of photons, thus, it can plague the S-to-N late in the pulse when the photon flux is low. Fig. 4 illustrates the problem. Shown are single gamma-ray and neutron pulses using the same crystal, but two different SiPMs with different afterpulsing characteristics. The SiPMs are two different models manufactured by Hamamatsu (HPK) (s12573-050 and s13360-6050). The manufacturer's listed afterpulsing probabilities (APP) are 2% and 0.1% respectively [10]. Note the better separation seen late in the pulse with the lower afterpulsing SiPM.

Fig. 5 shows PSD density contour plots similar to Fig. 2 but showing the difference between two SensL brand SiPMs also with different published APPs. Figs 2a and 2b show a SensL MicroB-60035 and a MicroJ-60035 having published APPs of 1% and 0.1%, respectively [11], [12]. The PSD FoMs are 1.16 and 1.89, respectively. Thus, the need for low after-pulsing SiPMs is paramount for the application of PSD to CLLB.

Table V lists performance data taken on the same crystal with various SiPMs from several different manufacturers. The edge of the crystal was optically coupled with silicone grease to the SiPMs as shown in Fig. 6a. For comparison, the last row

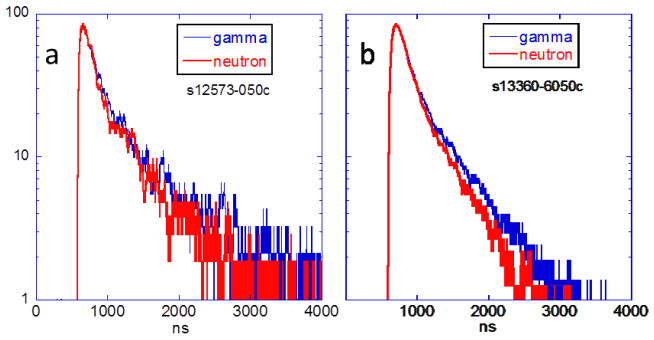


Fig. 4. Gamma and neutron pulses from SiPMs with different afterpulsing characteristics. a) pulses from an SiPM with 2% afterpulsing probability. b) pulses from an SiPM with 0.1% afterpulsing probability.

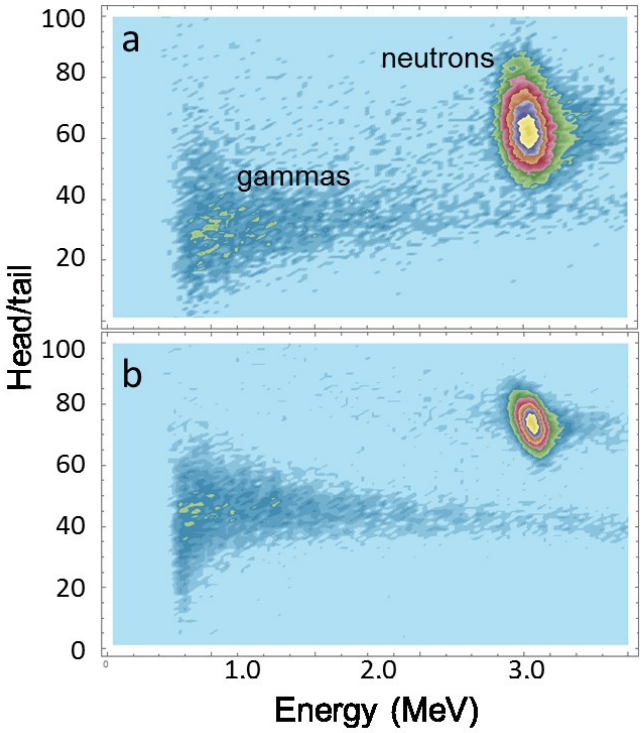


Fig 5. PSD density contour plots for the same CLLB crystal measured by two SiPMs with different afterpulsing characteristics. a) pulses from an SiPM with 1% afterpulsing probability. b) pulses from an SiPM with 0.1% afterpulsing probability. The PSD FoMs are 1.16 and 1.89 for a) and b), respectively.

of Table V contains data taken on a high quality PMT. The best results for energy resolution and PSD both come from the same SiPM, the SensL MicroJ-60035. Not surprisingly, this SiPM also has presently the best advertised photon detection efficiency, lowest dark count rate, and is equal to the best APP of all those tested. In some cases the SiPM used was not the latest model from that manufacturer. It is noted that SiPM technology is advancing rapidly, and these data may not reflect the best current performance available from a given manufacturer.

The best achieved energy resolution at 1275 keV is 4.4%. This may seem high when compared to published energy resolution values less than 3% at 662 keV. The main reason for the difference is the unfavorable geometry of placing a small area sensor on a large area scintillator. The average photon must travel a relatively long path around the inside of the crystal before it randomly intersects with the read-out SiPM. Long path lengths mean greater variance in the number of interactions with the (imperfect) reflector and in the number of optical absorptions in the bulk crystal. Tables IV and V illustrate this effect nicely: the smaller the sensor, the greater the pathlengths, and the worse the non-uniformity and energy resolution.

TABLE V. PERFORMANCE DATA FOR VARIOUS SIPMS

| Vendor | model | Dim. ($mm^2$) | Cell size (μm) | Energy resolution at 1275 keV | PSD FoM |
|---|---|---|---|---|---|
| SensL | B30035 | 3x3 | 35 | 8.9% | 0.8 |
| SensL | B60035 | 6x6 | 35 | 6.9% | 1.2 |
| SensL | C60035 | 6x6 | 35 | 4.9% | 1.9 |
| SensL | J60035 | 6x6 | 35 | 4.4% | 1.9 |
| HPK | 12572 | 3x3 | 15 | 8.3% | too poor |
| HPK | 12572 | 3x3 | 25 | 7.5% | 0.6 |
| HPK | 12572 | 3x3 | 50 | 6.9% | 1.1 |
| HPK | 12573 | 6x6 | 25 | 9.5% | too poor |
| HPK | 12573 | 6x6 | 50 | 9.4% | 0.9 |
| HPK | 13360 | 6x6 | 25 | 5.4% | 1.3 |
| HPK | 13360 | 6x6 | 50 | 5.1% | 1.5 |
| Ketek | PM33 | 3x3 | 50 | 7.0% | 1.0 |
| AdvanSiD | NUV-3S-P-4x4TD | 12x12 | 40 | 6.0% | 1.5 |
| HPK | R6233PMT | 6x6 (apertured) | | 3.6% | 2.0 |

The final design parameters of the compact gamma / neutron detector are

[Ce] = 2 mol.%
shape: disk
size: Ø = 52 mm, h = 6 mm
SiPM model: SensL MicroJ60035
SiPM placement: disk edge
γ/n algorithm: head-to-tail ratio of scintillation pulse

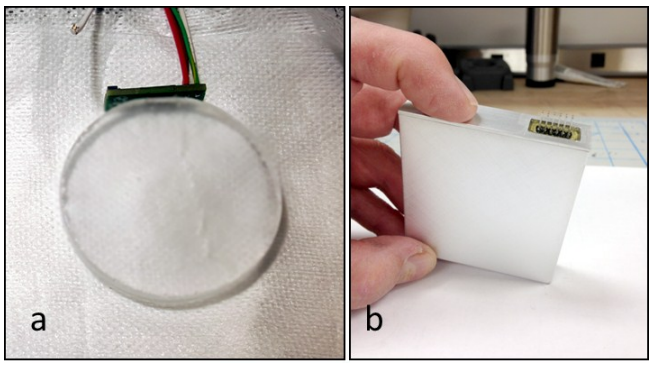


Fig. 6. a) photo of a bare CLLB disk coupled to a SiPM. For measurements, the crystal is wrapped with PTFE reflector. b) the crystal and SiPM are packaged in an aluminum housing suitable for output to a multichannel analyzer or other standard device.

In terms of a gamma-ray spectrometer, this CLLB detector has a detection capability equal to a NaI(Tl) crystal with dimensions, Ø=2.5 cm, h=2.5 cm and coupled to a PMT.

Detection capability is defined as the $^{137}Cs$ photopeak efficiency in counts/(s-mCi) at a 1 m distance from the source divided by the energy resolution in %fwhm. This metric gives an indication of how quickly an isotope can be identified based on gamma ray spectral peaks. This value is 45 cps/(mCi-%). In terms of a neutron detector, this CLLB detector has a thermal neutron detection efficiency of 0.06 cps/(ng of $^{252}Cf$) at a 1 m distance from the source and moderated with 5 cm of high density polyethylene. This is equivalent in efficiency to an $^{3}He$ tube with Ø=1.3 cm, h=5 cm, and pressure=8 atm. Fig. 6b is a photo showing the crystal in Fig. 6a housed in a 68 $cm^3$ aluminum case.

## III. Summary

A CLLB scintillator disk can be coupled to a small area SiPM and creates a suitable, compact, dual gamma ray spectrometer and neutron detector. The achieved results are gamma ray energy resolutions of 6.0% and 4.4% at 662 and 1275 keV, respectively, and a n/γ PSD FoM of 1.9. The proposed disk size of Ø=52 mm, h=6 mm will result in a 74% detection efficiency of incident thermal neutrons when the CLLB contains 95% enriched $^{6}Li$. The dimensions of the crystal enclosure are 7.0 x 6.5 x 1.5 $cm^3$, which allows an additional 180 $cm^3$ for the remaining electronics to keep the total volume under the desired 250 $cm^3$. The incorporation of the detector electronics is the subject of future work. The detector electronics will include on-board gamma and neutron count rates and energy spectra, PSD, temperature compensation, and gain stabilization.

## Acknowledgment

We thank M. Momayezi of Bridgeport Instruments LLC and M. Baginski of Sanmina-SCI Corp. for valuable input regarding the detector design.

## References

[1] U. Shirwadkar, J. Glodo, E. V. D. van Loef, R. Hawrami, S. Mukhopadhyay, A. Churilov, W. M. Higgins, K. S. Shah, "Scintillation properties of $Cs_2LiLaBr_6$ (CLLB) crystals with varying $Ce^{3+}$ concentration," Nucl. Instr. and Meth. A, vol. 652, pp. 268-270, 2011.

[2] J. Glodo, E. V. D van Loef, R. Hawrami, W. M. Higgins, A. Churilov, U. Shirwadkar, and K. S. Shah, "Selected Properties of $Cs_2LiYCl_6$, $Cs_2LiLaCl_6$, and $Cs_2LiLaBr_6$ Scintillators," IEEE Trans. Nuc. Sci, vol. 58, no.1, pp. 333-338, 2011.

[3] K. Yang, P. R. Menge, J. J. Buzniak, V. Ouspenski, "Scintillation properties and temperature responses of $Cs_2LiLaBr_6:Ce^{3+}$," Nuclear Science Symposium and Medical Imaging Conference, 2012 IEEE, pp. 308 – 311.

[4] R. A. Winyard, J. E. Lutkin and G. W. McBeth, "Pulse shape discrimination in inorganic and organic scintillators," Nucl. Instr. and Meth., vol. 95, no. 1, pp. 141-153, 1971.

[5] J. Glodo, R. Hawrami, E. V. D. van Loef, U. Shirwadkar, and K. S. Shah, "Pulse shape discrimination with selected elpasolite crystals," IEEE Trans. Nuc. Sci., vol. 59, no. 5, pp. 2328-2333, 2012.

[6] G.F. Knoll, T.F. Knoll and T.M. Henderson, "Light collection in scintillation detector composites for neutron detection," IEEE Trans. Nuc. Sci., vol. 35, pp. 872, 1988.

[7] F. Cayouette, D. Laurendeau, and C. Moisan, "DETECT2000: An improved Monte-Carlo simulator for the computer aided design of photon sensing devices," in Proc. SPIE Photonics North, Quebec, Canada, Jun. 2002.

[8] M. Moszynski, J. Zalipska, M. Balcerzyk, M. Kapusta, W. Mengesha, and J. D. Valentine, "Intrinsic resolution of NaI(Tl)," Nucl. Instrum. Methods Phys. Res. A, vol. A484, no. 1–3, pp. 259–269, May 2002.

[9] S. Cova, A. Lacaita, G. Ripamonti, "Trapping phenomena in avalanche photodiodes on nanosecond scale," IEEE Electron Devices Lett., vol. 12, no. 12, pp. 685-687, 1991.

[10] Hamamatsu.com, "MPPC and MPPC module for precision measurement," 2015. [Online]. Available: http://hamamatsu.com/resources/pdf/ssd/mppc_kapd0002e.pdf. [Accessed: 13- Nov- 2015].

[11] K. O'Neill and C. Jackson, "SensL B-Series and C-Series silicon photomultipliers for time-of-flight positron emission tomography," Nuc. Instrum. and Meth. A, vol. 787, pp. 169-172, 2015.

[12] Sensl.com, "J-Series High-Density Fill Factor Silicon Photomultipliers," 2015. [Online]. Available: http://sensl.com/downloads/ds/DS-MicroJseries.pdf. [Accessed: 13- Nov- 2015].